# Cobalt Catalysts Decorated with Platinum Atoms Supported on Barium Zirconate Provide Enhanced Activity and Selectivity for $CO_2$ Methanation

Hyun Ho Shin,[†] Li Lu,[‡] Zhou Yang,[†] Christopher J. Kiely,[†,‡] and Steven McIntosh[*,†]

[†]Department of Chemical and Biomolecular Engineering and [‡]Department of Materials Science and Engineering, Lehigh University, Bethlehem, Pennsylvania 18015, United States

[*] Supporting Information

ABSTRACT: A perovskite-structured barium zirconate, $BaZrO_3$ (BZ), support is demonstrated to enhance the activity, relative to γ-$Al_2O_3$, of Co nanoparticle catalysts decorated with Pt for $CO_2$ methanation. The $CO_2$ methanation reaction may play a central role in both $CO_2$ utilization and energy storage strategies for renewable energy. These catalysts require cooperative hydrogen transport between the supported Pt and Co species to provide the desired functionality, as $CO_2$ preferentially dissociates on Co with $H_2$ dissociating primarily on Pt. In this work, this interaction is enhanced through an atomic decoration of Pt on the Co nanoparticle surface. This morphology is achieved through immobilization of colloidal Pt particles on the Co/$BaZrO_3$ support followed by selected catalyst pretreatment conditions to atomically disperse the Pt. Furthermore, at the same loading of Co and Pt (1 and 0.2 wt %, respectively), the barium zirconate support provides a more than 6-fold increase in $CH_4$ formation rate in comparison to previously studied γ-$Al_2O_3$ supports at 325 °C. This was accompanied by a $CH_4$ selectivity of over 70%, which was maintained over the measured temperature range of 250−350 °C; in fact, the selectivity was 80% at 325 °C, in comparison to only 43% for γ-$Al_2O_3$ support. This enhancement is attributed to a strong interaction between the Co particles and the $BaZrO_3$ support. Yttria doping at 5 and 30 atom % levels on the zirconia site led to a reduction of the catalytic performance relative to $BaZrO_3$, although the activity displayed at low levels of substitution was still higher than that over the γ-$Al_2O_3$ support.

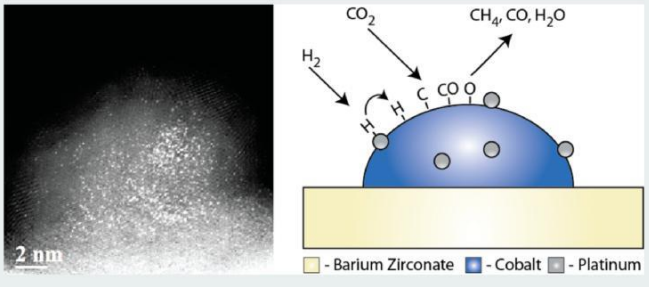


KEYWORDS: carbon dioxide methanation, hydrogenation, Co−Pt catalysts, barium zirconate perovskite, γ-alumina, metal support wetting interaction, hydrogen spillover, atomically dispersed Pt

## INTRODUCTION

Reduction of carbon dioxide ($CO_2$) is of increasing interest as a route to decrease the impact of anthropogenic greenhouse gases on climate.[1,2] $CO_2$ methanation can effectively utilize $CO_2$ emissions while simultaneously generating a substitute hydrocarbon fuel,[3] potentially closing a carbon fuel emission cycle.[4] This reaction may also play an essential future role in enabling large-scale storage of energy produced from renewable sources by utilizing hydrogen produced via electrolysis to convert $CO_2$ to methane fuel. This methane may then be stored in the existing natural gas infrastructure. Nanostructured cobalt-based catalysts have previously been identified as active for hydrogenation,[5−8] particularly when promoted by separate particles of platinum and other precious metals.[9,10]

Advances in nanoscience have led to significant advances in our ability to design, control, implement, and understand heterogeneous catalysts at the smallest scale, even down to single atoms.[11−15] With reference to $CO_2$ and CO hydro-genation, elegant kinetic studies by the Somorjai group utilizing both size- and morphology-controlled cobalt and platinum nanoparticles supported on mesoporous silica have focused on understanding the reaction mechanism, the effect of catalyst particle size, and the introduction of a promoter such as Pt.[16−18] These studies indicated that a mixture of size-controlled nanoparticles of pure Co and Pt yields a significant enhancement in $CO_2$ methanation rate in comparison to Co−Pt bimetallic nanoparticles. The reaction pathway involved a cooperation between the two metals; $CO_2$ dissociation occurs on the Co particles, with $H_2$ dissociation occurring on Pt. The reaction is thought to proceed via hydrogen spillover from the Pt nanoparticles onto the oxide support, followed by surface migration of the hydrogen atoms to the Co nanoparticles and subsequent formation of methane. The observed significant drop in apparent activation energy upon the addition of Pt nanoparticles implies that the rate-limiting mechanistic step is the surface migration of hydrogen from Pt to Co.[18]

Acceptor-doped $BaZrO_3$ and $BaCeO_3$ ceramics are of interest as proton conducting materials for solid oxide fuel cell

electrolytes.[19] This application utilizes the incorporation of mobile protons into the bulk of these perovskite structured oxides. In addition to such fuel cell focused studies, we have recently investigated the reaction kinetics of proton incorporation[20] and the potential of utilizing these materials as catalyst support materials.[21] Of considerable interest is the possible use of this class of materials as oxide supports for metal-catalyzed hydrogenation and dehydrogenation reactions.

We have previously demonstrated a significant rate enhancement for Cr-catalyzed nonoxidative ethane dehydrogenation when utilizing perovskite-structured $BaCeO_3$ and $BaZrO_3$ supports.[21] These support materials lead to more than 1 order of magnitude improvement in ethylene formation rate in comparison to $\gamma$-$Al_2O_3$.[21] This enhancement in catalytic activity was attributed to possible proton incorporation in the perovskite supports through hydrogen spillover from chromium.[20] Our previous work to measure $H_2/D_2$ exchange kinetics over these materials demonstrated that yttria-doped $BaCeO_3$ and $BaZrO_3$ can rapidly exchange significant quantities of H for D: up to 13% of all bulk protons.[3]

In this current work, we investigate the use of $BaZrO_3$, $BaZr_{0.95}Y_{0.05}O_{3-\delta}$, and $BaZr_{0.8}Y_{0.2}O_{3-\delta}$ oxide supports to enhance the activity and selectivity of Co nanoparticle catalysts decorated with Pt for $CO_2$ methanation. HAADF-STEM studies demonstrate that Pt migration during catalyst pretreatment leads to decoration of the Co nanoparticle, and possibly the support material, with Pt atoms. When this process is coupled to a significant Co−support interaction, as evidenced by significant wetting of the support, this yields a 6-fold increase in reaction rate for $CO_2$ methanation on $BaZrO_3$ in comparison with a $\gamma$-$Al_2O_3$ support. This rate increase is coupled with a significant increase in $CH_4$ vs CO selectivity.

## EXPERIMENTAL SECTION

Co nanoparticles were prepared by a Schlenk technique under an argon atmosphere following a previously reported procedure.[16] A 1.025 g portion of cobalt carbonyl (Sigma, moistened with 1−10% hexane, 99.3% Co) was dissolved in 6 mLof 1,2-dichlorobenzene (Sigma, 99%). All handling of $Co_2(CO)_8$ was carried out in a glovebox under $N_2$. A 0.3 mL portion of oleic acid (Alfa Aesar, 90%) and 30 mL of 1,2-dichlorobenzene (DCB) were placed in a 100 mL three-neck flask. The solution was degassed for 20 min and then stirred under argon for another 20 min prior to heating to 170 °C. The $Co_2(CO)_8$ in DCB (0.5 M) was rapidly injected under vigorous stirring conditions, leading to a rapid color change to black, indicating formation of colloidal Co nanoparticles. This solution was kept at 170 °C for 20 min and then cooled to 50 °C. Co nanoparticles were precipitated by adding 20 mL of DCB and 40 mL of 2-proponal (ACS grade), followed by centrifugation (8000 rpm). The precipitated solid was redispersed and stored in chloroform (ACS grade) until required for use.

Pt nanoparticles were prepared following a procedure reported in the literature.[22] An 80 mg portion of platinum(II) acetylacetonate ($Pt(acac)_2$, Alfa Aesar, ≥48% Pt, total metal impurities <0.04%) was added to 10 mL of 1-octadecene (Alfa Aesar, 90%) mixed with 1 mL of oleic acid (Alfa Aesar, 90%) and 1 mL of oleylamine (Sigma, 98%). The solution was degassed for 20 min and then stirred under argon for another 20 min. Under conditions of vigorous stirring, the solution was slowly heated to 120 °C and kept there for 30 min to dissolve the $Pt(acac)_2$. The temperature was further raised to 200 °C, and the yellow solution turned black, indicating the formation of colloidal Pt nanoparticles. This solution was held at 200 °C for 30 min and then cooled to room temperature. Pt nanoparticles were precipitated by adding 20 mL of acetone (semiconductor grade) and 20 mL of methanol (semiconductor grade), followed by centrifugation (8000 rpm). The precipitated solid was redispersed and stored in chloroform (ACS grade) until required for use.

As supports for Co or Pt particles in the $CO_2$ methanation reaction, $BaZrO_3$, $BaZr_{0.95}Y_{0.05}O_{3-\delta}$, and $BaZr_{0.8}Y_{0.2}O_{3-\delta}$ were synthesized utilizing a modified Pechini method. Aqueous solutions of $Ba(NO_3)_2$, $Zr(NO_3)_2$, and $Y(NO_3)_2$ (>99% pure, Alfa Aesar) were prepared, and the metal concentrations were determined by redox titration.[23] The solutions were mixed, in the stoichiometric ratio needed to fabricate the desired composition, with the chelating agent EDTA (99%, Alfa Aesar) and citric acid monohydrate (99.0−102.0%, Alfa Aesar). The pH was adjusted to >8.5 by addition of ammonium hydroxide (14.8 N, Fisher Scientific). After the excess water was evaporated, the resulting homogeneous gel was combusted in an oven at 300 °C, and the powder generated was sintered for 4 h at 1300 °C. Colloidally prepared metal nanoparticles were supported on the synthesized pure oxide (either 1.0 wt % Co, 1.0 wt % Pt, or 1.0 wt % Co + 0.2 wt % Pt, respectively denoted as 1Co, 1Pt, or 0.2Pt1Co hereafter) using a standard incipient wetness procedure[20,24] where chloroform was utilized as the solvent. The samples were placed in a muffle furnace in air and held at 500 °C for 1 h prior to use. For comparative purposes, Co and Pt supported on $\gamma$-$Al_2O_3$ were also prepared by incipient wetness (>99% pure, Alfa Aesar). All of the catalysts were prepared from the same stock solutions of Co and Pt nanoparticles with loadings calculated from the concentration of nanoparticles in solution.

The synthesized materials were characterized by powder X-ray diffraction with Cu Kα radiation and fixed slit width (MiniFlex (II), Rigaku). Diffraction patterns were recorded in the 2θ range of 20−70° with a step size of 0.02° and a counting time of 0.2 min/deg. The BET surface area was measured (ASAP2020, Micromeritics) using krypton gas as the absorbent after samples were degassed at 300 °C for 10 h. Scanning transmission electron microscopy (STEM) imaging was conducted at 200 kV using an aberration-corrected JEOL ARM 200CF microscope equipped with a JEOL Centurio XEDS system. Co and Pt nanoparticle samples were prepared by drop-casting the colloidal solution onto a carbon-coated copper TEM grid and allowing the liquid component to fully evaporate. Prior to STEM imaging, the as-prepared supported metal catalyst was oxidized to remove surface contaminants at 500 °C for 1 h in a flow of 50 mL/min 19.5−23.5 vol % $O_2/N_2$ (99.999%, GTS-Welco) and then reduced at 450 °C under flowing 10 vol % $H_2$/Ar (99.999%, <1 ppm of $O_2$, GTS-Welco) for 1 h. These are the same conditions used to pretreat the catalyst prior to measuring catalytic activity. The Co/Pt/$BaZrO_3$ catalyst samples were prepared for STEM analysis by dry-dispersing the powder onto a holey carbon grid.

X-ray photoelectron spectroscopy (XPS) measurements were performed to investigate the oxidation state of the nanoparticulate Co supported on $BaZrO_3$ and $Al_2O_3$. Prior to XPS measurements, samples were pretreated by the same oxidation/reduction procedure described above for TEM sample preparation. The samples were mounted on double-sided carbon tape and transferred to a sample holder. No signal from the carbon tape was detected by XPS. The spectra were

obtained on a Thermo Scientific K-Alpha instrument with a monochromated Al Kα X-ray source of 1486.6 eV energy. The beam footprint on the sample was an ellipse with a major axis of 400 μm and a minor axis of 250 μm.

$CO_2$ methanation was performed with sieved powder catalyst (106−150 μm) as a fixed bed in a continuous flow quartz tube reactor (i.d. 4 mm, length of 300 mm). The 0.2 g catalyst sample was held in place by quartz glass wool. Gas flows were regulated by mass flow controllers (4850 series, Brooks). Prior to measurement, the samples were heated to 500 °C at a rate of 10 °C/min in a flow of 100 mL/min dry air containing <0.5 ppm of $CO_2$ and then held for 1 h at this temperature to remove moisture and contaminants on the surface of the catalyst that may have accumulated during storage. The powder sample was then cooled to 450 °C under the same flow conditions and subsequently reduced at 450 °C for 1 h under a 5 vol % $H_2/N_2$ mixture flowing at 50 mL/min. This pretreatment temperature has been previously indicated as sufficient to reduce cobalt oxide nanoparticles to cobalt metal.[6] Omission of the reduction step led to an inactive catalyst. The reactor was flushed with Ar and cooled to the desired reaction temperature after this pretreatment, prior to feeding in the reactant mixture of 3 vol % $CO_2$ and 9 vol % $H_2$ balanced with Ar (99.999%, <1 ppm of $O_2$, GTS-Welco) at 100 mL/min at the reaction temperature. This procedure was repeated, and the reaction was carried out at 25 °C temperature intervals between 200 and 350 °C.

The initial concentrations of reactant, $CO_2$ (m/e 44), and products, CO (m/e 28) and $CH_4$ (m/e 16), were monitored (sampling frequency 1.67 $s^{-1}$) for 10 min at each reaction temperature using a residual gas analyzer (RGA) fitted with a quadropole mass analyzer and associated Faraday and secondary electron multiplier detectors (Cirrus 2, MKS Instruments UK Ltd.). The amount of deposited carbon was determined from the amount of $CO_2$ generated as calculated from numerical integration of the area under the $CO_2$ peak. The $CO_2$ peak area was calibrated by using a 100 μL pulse of $CO_2$. Temperature-programmed oxidation of the as-tested catalyst was also performed by heating from room temperature to 600 °C at 10 °C/min in a 100 mL/min flow of dry air containing <0.5 ppm of $CO_2$.

## RESULTS

Phase pure $BaZrO_3$, $BaZr_{0.95}Y_{0.05}O_{3-\delta}$, and $BaZr_{0.8}Y_{0.2}O_{3-\delta}$ were synthesized. X-ray diffraction patterns were indexed to a cubic perovskite structure (space group $Pm\bar{3}m$) for $BaZrO_3$ and $BaZr_{0.95}Y_{0.05}O_{3-\delta}$[25−27] and to a tetragonal structure (P4mm) for $BaZr_{0.8}Y_{0.2}O_{3-\delta}$[28,29] (Figure S1 in the Supporting Information). Scanning transmission electron microscopy of as-prepared colloidal Pt and Co nanoparticles demonstrate that the mean diameters of Pt and Co are ~2.5 and ~12.0 nm, respectively (Figure 1a,b). These particles were prepared utilizing the same procedures reported in previous $CO_2$ methanation studies.[16,18] The inset in Figure 1a shows that the as-prepared Pt particles are highly crystalline, in this case showing the [110] projection of FCC Pt. The as-prepared Co particles show a distinct core− shell structure with a sharp transition from a lower intensity shell to a brighter core in the HAADF-STEM images. This is consistent with a 6 nm diameter metallic Co core surrounded by a 3 nm thick Co oxide shell. Higher resolution imaging (see Figure 1c and Figures S2−S4 in the Supporting Information) indicates a crystalline HCP core surrounded by a polycrystalline

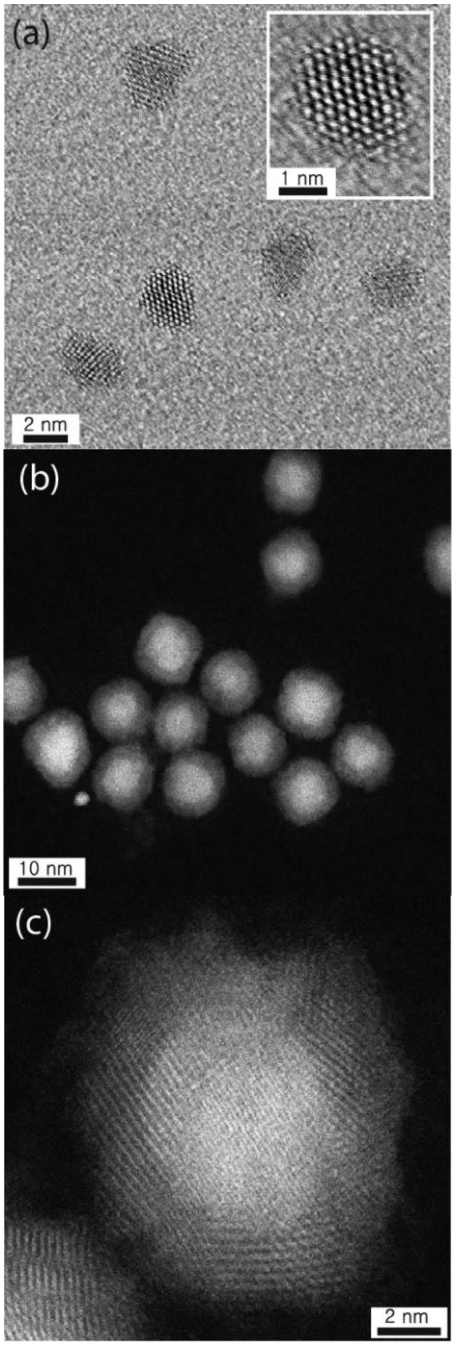


Figure 1. (a) BF-STEM image of as-prepared Pt nanoparticles and (b, c) HAADF-STEM images of as-prepared Co nanoparticles showing a distinct core−shell structure.

Co oxide shell. This oxidation may be due to exposure of the sample to air prior to insertion into the electron microscope.

All of the catalyst loadings reported in this paper correspond to weight loadings of the metal nanoparticles. The supported 0.2 wt % Pt + 1 wt % Co/γ-$Al_2O_3$ material following calcination in air at 500 °C and reduction at 450 °C in 10 vol % $H_2$/Ar is shown in Figure 2. Figure 2a is a BF-STEM image of a Co particle on the support, showing a high contact angle between Co and γ-$Al_2O_3$ indicative of limited wetting of the support by Co (see also Figure S5 in the Supporting Information). The Co oxide shell−Co core motif observed in the as-prepared Co particles is similarly observed in the supported particles. Again, this may be due to oxidation upon transfer of the catalyst

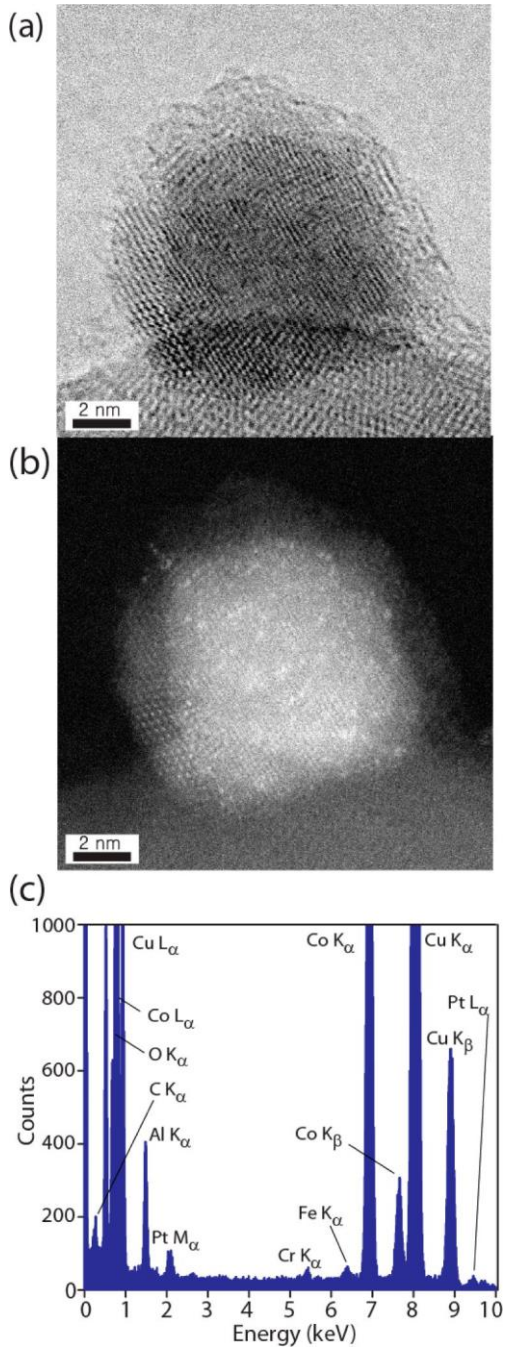


Figure 2. Complementary (a) BF-STEM and (b) HAADF-STEM images of a Co particle supported on $Al_2O_3$ after calcination at 500 °C in air and reduction at 450 °C in 10 vol % $H_2$/Ar. (c) XEDS spectrum collected from the supported particle.

sample to the microscope in air. On the basis of previous reports for 10 nm Co nanoparticles, a sample reduction temperature of 450 °C is expected to be sufficient to fully reduce the Co prior to reaction.[6] Lattice fitting for the oxide shell of the particles supported on γ-$Al_2O_3$, and $BaZrO_3$ discussed below, indicates that the shell consists of a mixture of the cubic spinel $Co_3O_4$, cubic rock salt CoO, and hexagonal $Co_2O_3$ phases (Figure S3 in the Supporting Information).

The corresponding HAADF-STEM image (Figure 2b) of the same particle clearly shows individual Pt atoms decorating the Co particle. The Pt atoms appear as isolated bright spots located on the Co/$CoO_x$ interface and are visible due to the higher atomic mass density of Pt relative to that of Co and O. These images are representative of all the Co particles observed. Since Pt is more noble than Co, it prefers to remain associated with the metallic Co core as opposed to being incorporated into the $CoO_x$ shell during oxidation of the particle. The location of the Pt on the surface of the hcp Co makes this structure distinct from a homogeneous Co−Pt alloy. The corresponding XEDS spectra (Figure 2c) confirms the presence of both metal atoms in a single particle. This sparse atomic decoration of Pt on the metallic Co particle surface is quite distinct from the structure of the bulk alloyed Pt−Co bimetallic particles previously studied by Beaumont et al.[17] for this reaction. A small number of individual Pt particles were also observed, but very little atomically dispersed Pt was found on the γ-$Al_2O_3$ support (Figure S6 in the Supporting Information).

Counting the individual Pt atoms observable on a number of Co particles yields between ~50 and 450 atoms. These Pt atoms, if reassembled, would give particles of between ~1.1 and 2.35 nm in diameter. Considering that some of the Pt atoms will be out of the plane of focus in the HAADF images, these Pt doping levels per Co nanoparticle are approximately in line with the number of Pt atoms expected to exist in individual nanoparticles deposited onto the catalyst.

Similarly, the 0.2 wt % Pt + 1 wt % Co/$BaZrO_3$ catalyst following calcination in air at 500 °C and reduction at 450 °C in 10 vol % $H_2$/Ar is shown in Figure 3. The BF-STEM image in Figure 3a shows a Co particle wetting the $BaZrO_3$ support material to form a low contact angle interface (see also Figure S7 in the Supporting Information). As with the other Co particles, a hemispherical polycrystalline Co oxide shell surrounding the exposed crystalline metallic Co core is clearly visible. Again, the reduction prior to reaction is expected to fully reduce the Co oxide shell to metallic Co.[6] The corresponding HAADF-STEM image (Figure 3b) once again clearly shows Pt atoms decorating the surface Co/$CoO_x$ interface within the nanoparticle. This is confirmed by the corresponding XEDS spectrum from a single Co particle (Figure 3c). As with the γ-$Al_2O_3$-supported catalyst, counting the approximate number of individual platinum atoms per Co particle yields values approximately equivalent to the number of Pt atoms present in individual as-prepared Pt nanoparticles. We were unable to obtain informative z-contrast images from the $BaZrO_3$ material to investigate if there is an atomic dispersion of Pt atoms due to the much greater thickness of the support; however, we consider that it is plausible that the $BaZrO_3$ crystallites may have some residual Pt atoms and Pt nanoparticles present on their surface.

XEDS spectra obtained from individual Co-rich nanoparticles in profile view (Figure 3c) confirms that the particles are primarily Co with a relatively small Pt content. However, as with imaging, no unambiguous Pt signal on the $BaZrO_3$ support could be detected by XEDS analysis due to the relatively small amount of Pt present, the overlap of the Pt Mα peak with the Zr Lα peak at around 2.05 keV, and the significant thickness of the support material.

XPS measurements were also performed to investigate the oxidation state of supported Co over $BaZrO_3$ and γ-$Al_2O_3$ (Figure S8 in the Supporting Information). The samples were pretreated in $H_2$ at 450 °C for 1 h prior to transfer in air to the XPS. The Co 2p and Co 3p spectra were fitted using peaks from reference samples in the Thermo Avantage Database. In

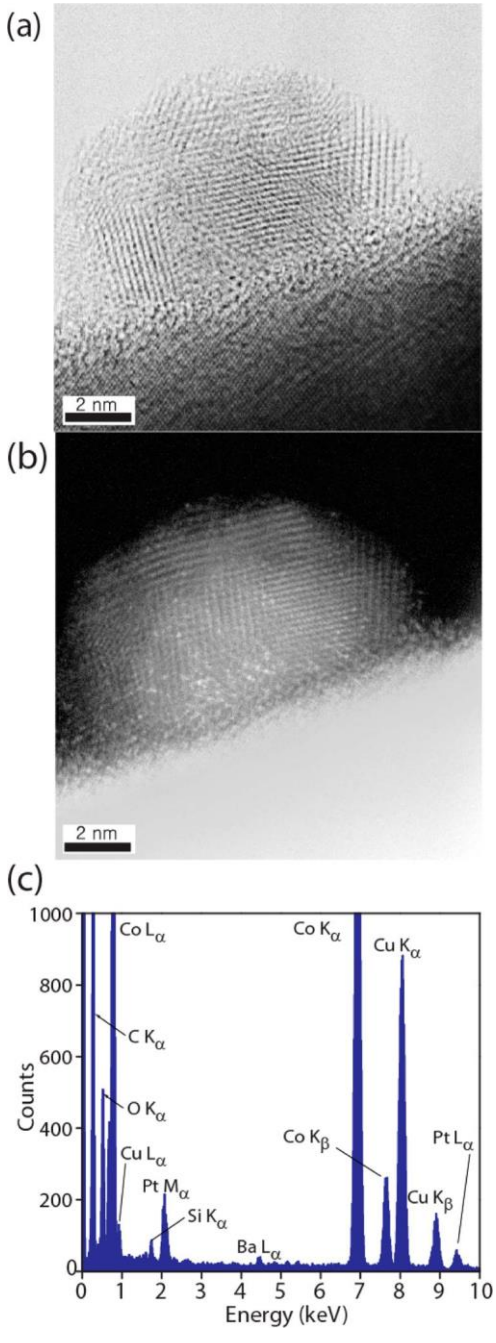


Figure 3. Complementary (a) BF-STEM and (b) HAADF-STEM images of a Co particle supported on $BaZrO_3$ after calcination at 500 °C in air and reduction at 450 °C in 10 vol % $H_2$/Ar. (c) XEDS spectrum collected from the supported particle.

the case of the 1Co/$BaZrO_3$ and 0.2Pt1Co/$BaZrO_3$ samples, the Co 2p region could not be analyzed due to the overlap of Co 2p and Ba 3d signals. The XPS spectra indicate that the Co component in all catalysts consists of a mixture of CoO and $Co_3O_4$ (i.e., no metallic Co was observed). This result is in good agreement with the STEM observations of a polycrystalline Co oxide shell surrounding a metallic Co core. The shell material of ~3 nm thickness essentially dominates the XPS signal. The formation of this oxide shell on the Co nanoparticles is once again most likely to occur during aerobic transfer to the XPS instrument.

The catalytic rates of $CH_4$ formation measured over 0.2 g of these catalysts between 200 and 350 °C are shown in Figure 4a.

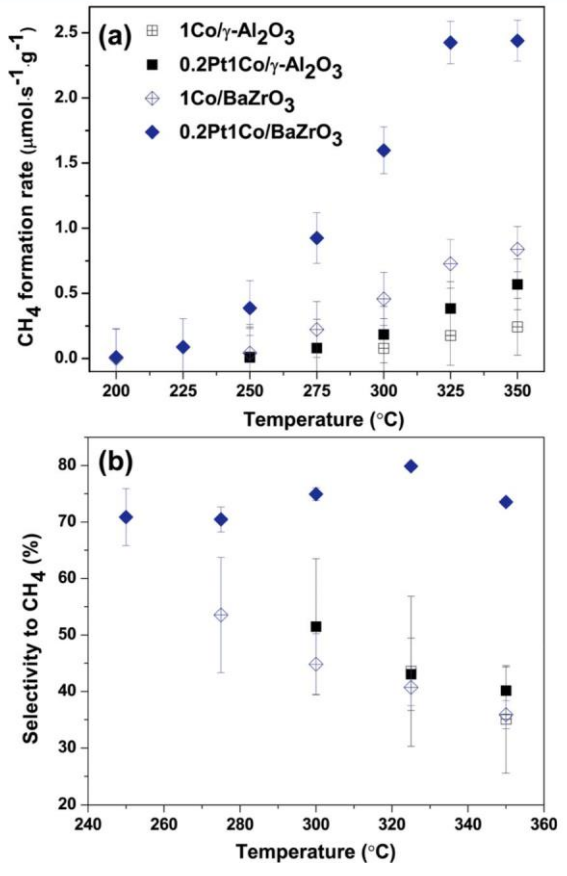


Figure 4. (a) $CH_4$ formation rate and (b) selectivity to $CH_4$ as a function of reaction temperature over 1Co/γ-$Al_2O_3$, 0.2Pt1Co/γ-$Al_2O_3$, 1Co/$BaZrO_3$, and 0.2Pt1Co/$BaZrO_3$ catalysts.

The rate was normalized by the total catalyst mass (Co, Pt, and support), because the same nominal Co and Pt mass loading was utilized for each catalyst sample and the active phase is homogeneously distributed over the support. Normalization based on support surface area would yield an apparent greater enhancement in rate for the lower surface area $BaZrO_3$ support. The specific surface areas of the γ-$Al_2O_3$ and $BaZrO_3$ materials are 54 and 2 $m^2$/g, respectively. No $CH_4$ formation and only minimal CO formation was observed when utilizing a Co-free 1Pt/$BaZrO_3$ catalyst under the same reaction conditions (Figure S9 in the Supporting Information). Turnover frequencies are comparable to those reported by Beaumont et al. utilizing a silica support[18] (Table S1 in the Supporting Information).

Gas-phase selectivity to $CH_4$, defined as the molar ratio of $CH_4$ to $CH_4$ + CO, was measured for each catalyst after 10 min on stream and is shown in Figure 4b. The only gas-phase species detected were $CH_4$, $CO_2$, CO, $H_2$, and $H_2O$. The selectivity to $CH_4$ of the γ-$Al_2O_3$ supported and 1Co/$BaZrO_3$ catalysts decreased with increasing temperature; for example, the $CH_4$ selectivities over 1Co/$BaZrO_3$ were 53.5, 44.8, 40.7 and 35.9% at 275, 300, 325, and 350 °C, respectively. In contrast, a high $CH_4$ selectivity over the 0.2Pt1Co/$BaZrO_3$ catalyst was maintained as the reaction temperature was increased, with a maximum of 80% being attained at 325 °C.

To investigate the possible role of bulk proton incorporation in these catalysts, Co- and Pt-containing catalysts were supported on $BaZrO_3$ doped with 5 and 20 atom % Y substituted onto the Zr site. Y doping of $BaZrO_3$ can be charge compensated by the incorporation of protons into the lattice.[30] Increasing the amount of Y dopant in the $BaZrO_3$ support results in a decrease of $CH_4$ formation rate and selectivity (Figure 5a,b), although all of the materials tested show rates

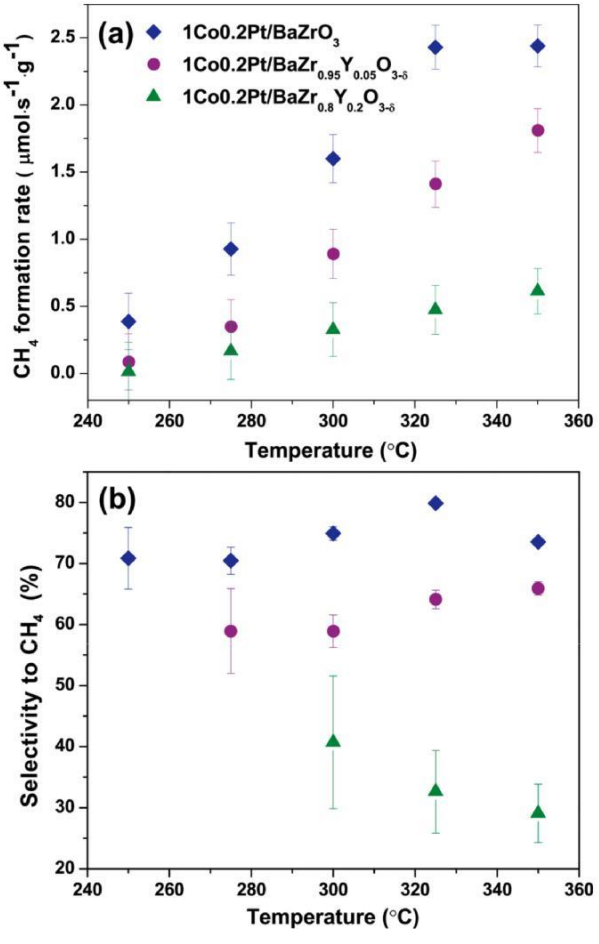


Figure 5. (a) $CH_4$ formation rate and (b) selectivity to $CH_4$ as a function of the reaction temperature over the 0.2Pt1Co/$BaZrO_3$, 0.2Pt1Co/$BaZr_{0.95}Y_{0.05}O_{3-\delta}$, and 0.2Pt1Co/$BaZr_{0.8}Y_{0.2}O_{3-\delta}$ catalysts.

higher than those observed for the γ-$Al_2O_3$ variants. The measured $CH_4$ formation rates were 2.4, 1.8, and 0.5 × $10^{-6}$ mol/(s g) for 0.2Pt1Co supported on $BaZrO_3$, $BaZr_{0.95}Y_{0.05}O_{3-\delta}$, and $BaZr_{0.8}Y_{0.2}O_{3-\delta}$, respectively, at 325 °C. The corresponding value for the 0.2Pt1Co/γ-$Al_2O_3$ catalyst is 0.4 × $10^{-6}$ mol/(s g).

A lifetime test was performed using the 0.2Pt1Co/$BaZrO_3$ material at 300 °C for 24 h and 350 °C for 3 h, respectively. The change in $CH_4$ formation rate and selectivity to $CH_4$ as a function of time are shown in Figure 6a. At 300 °C for 24 h, the catalyst performance gradually degraded to 66.6% of the initial $CH_4$ formation rate and 65.8% of the initial selectivity to $CH_4$. For the sample used at 350 °C for 3 h, the $CH_4$ formation rate and selectivity rapidly decreased to 25.9% and 42.5% of their initial values, respectively. Figure 6b shows the results of temperature-programmed oxidation of 0.2Pt1Co/$BaZrO_3$ catalyst tested for 3 h at 300 and 350 °C and for 24 h at 300 °C. $CO_2$ evolution was clearly observed as a single peak with a

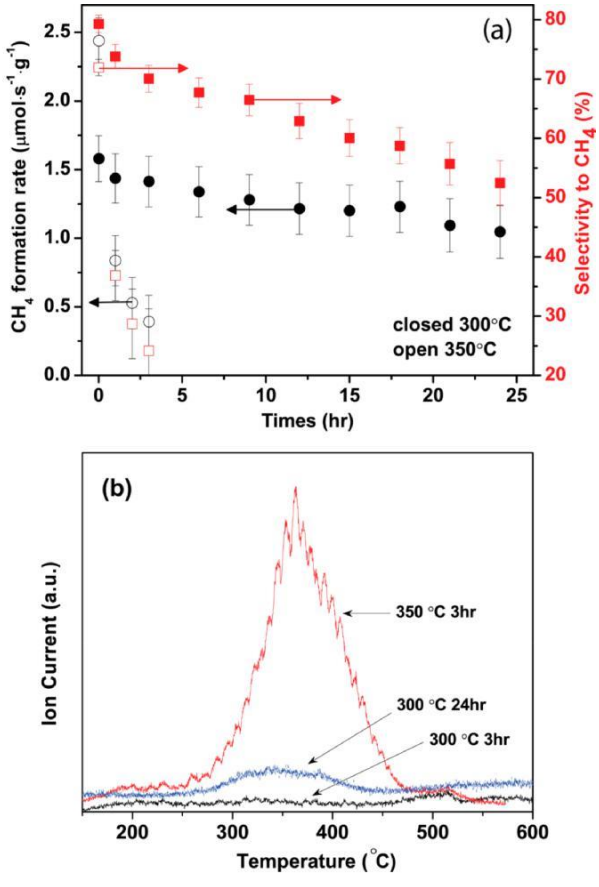


Figure 6. (a) $CH_4$ formation rate versus time over the 0.2Pt1Co/$BaZrO_3$ catalyst at 300 and 350 °C. (b) Subsequent temperature-programmed oxidation of the 0.2Pt1Co/$BaZrO_3$ catalyst after testing for 3 and 24 h at 300 °C and for 3 h at 350 °C.

maximum occurring at 380 °C for the catalyst used at ~360 °C. While no $CO_2$ evolution was observed after 3 h at 300 °C, a relatively small peak again centered at ~360 °C was observed after 24 h on stream. These results confirm that carbon deposition is the likely cause of the rapid deactivation when operating at 350 °C and slower deactivation at 300 °C. Furthermore, the low oxidation temperature of the deposited carbon suggests that this carbon is not graphitic in character. The calculated number of deposited C atoms per Co atom was 0.4 when testing was carried out at 350 °C for 3 h. Assuming a constant deposition rate, we estimate a carbon deposition rate of 1.5 × $10^{-2}$ μmol/(s g), which is significantly lower than the observed reaction rates. This low deposition rate could not be accurately determined by carbon balance during the reaction. This deactivation by carbon deposition is consistent with the observed constant decline in rate of $CH_4$ production over 0.2Pt1Co/$BaZrO_3$ between 300 and 350 °C, as shown in Figure 6a.

## DISCUSSION

The increased $CH_4$ production rate noted upon addition of Pt to supported Co is in agreement with the prior reports of a co-operative methanation reaction mechanism involving both Co and Pt nanoparticles.[17,18] These previous reports suggest a mechanism whereby $H_2$ dissociation occurs on isolated Pt nanoparticles, with $CO_2$ dissociation occurring on spatially separated Co nanoparticles. This then requires a proposed rate-limiting hydrogen spillover and transport step from the Pt to

the Co in order to form $CH_4$. The lack of $CH_4$ formation activity in the absence of Co nanoparticles further corroborates the concept that Co is necessary for $CO_2$ activation. Our previous isotopic exchange measurements[3] demonstrated much more facile hydrogen dissociation over $Pt/BaZrO_3$ in comparison to $Co/BaZrO_3$,[20] supporting the concept that $H_2$ dissociation primarily occurs on the Pt nanoparticles. However, in our catalysts, the Pt does not exist as individual nanoparticles but rather atomically decorates the Co nanoparticle surface.

Figures 2 and 3 demonstrate that, while we may initially have isolated Pt and Co nanoparticles, the catalyst pretreatment step leads to migration of Pt to decorate the Co particle surface. The counting of individual Pt atoms on the catalysts suggests that this decoration occurs from dispersion of the atoms in individual Pt nanoparticles initially in close proximity to, or even on, the individual Co particles. It is also possible that Pt atoms decorate the $BaZrO_3$ family of supports; however, we could not directly image these on the $BaZrO_3$ due to the high thickness of the support grains nor could we unambiguously identify them via XEDS analysis due to their low concentration. We do not, however, see any significant amount of atomically dispersed Pt on the γ-$Al_2O_3$ supports.

The migration of these small Pt particles is likely due to the relatively high calcination (500 °C) and reduction (450 °C) temperatures employed during catalyst pretreatment in the current study. While bulk Pt melts at 1768 °C, metal nanoparticles are known to exhibit significant melting point depressions.[31] Calculation of the Pt melting point with particle size indicates that a 2−3 nm Pt particle will melt between 950 and 1438 °C depending on the method of parameter estimation.[32] Thus, the catalyst calcination temperature is between one-third and one-half of the melting point of the Pt nanoparticles (i.e., above the Huttig temperature for surface diffusion but below the Tammann temperature for bulk diffusion), supporting the concept that significant Pt migration occurs during pretreatment. Similar calculations for the larger Co particles yields expected melting points of between 1370 and 1382 °C, explaining their relative stability and observed extended intimate low contact angle interface with the support. We also note that, while prior studies examined the role of 1.8 nm Pt particles in reducing Co, they only reported rates and mechanism for 12 nm Pt particles.[13] These larger Pt particles will undoubtedly be considerably more stable during sample pretreatment.

The Pt decoration observed in this study does not completely negate the previously proposed mechanism of hydrogen transport from spatially separated Pt to Co nanoparticles; however, for our catalysts, it does indicate a perhaps more significant role for spillover from Pt that is in close proximity to, and even "on", the Co phase. The increase in observed $CH_4$ rate and selectivity suggests that the atomic decoration of Pt leads to enhanced availability of hydrogen in intimate contact with the dissociated $CO_2$ on the Co surface.

The change from the γ-$Al_2O_3$- to the $BaZrO_3$-based supports leads to a significant increase of both methane production rate and $CH_4$ selectivity. The lack of $CH_4$ formation on the Co-free $1Pt/BaZrO_3$ indicates that the observed rate enhancement for the $BaZrO_3$ support is not due to any discrete Pt nanoparticles that may exist on the $BaZrO_3$ surface but that cannot be detected by HAADF-STEM imaging. The Pt decoration of the Co nanoparticles does not appear to vary with support identity; however, STEM analysis shows a clear difference in Co particle wetting behavior on the supports. While there is minimal wetting on the γ-$Al_2O_3$ grains, Co on $BaZrO_3$ forms a low contact angle interface. This stronger interaction between Co and the $BaZrO_3$ support is a potential factor contributing to the significant difference in activity and selectivity between support materials and may indicate that the perimeters of the Co particles play a significant role in the catalysis. It is likely that this influences the activity of both the Co and the decorating Pt atoms.

Such support-dependent structural changes, often encompassed by the term strong metal−support interactions, are frequently reported to substantially influence the catalytic activity of supported metal catalysts.[33−37] The change in activity is typically ascribed to one or more of the following: (a) changes in particle morphology, (b) electronic interactions between metal and support, or (c) the creation of active sites at the metal/support interface. With direct relevance to the current work, Riva et al. demonstrated more significant spreading of Co on $TiO_2$ in comparison to that of Co on a $SiO_2$ support.[38] This phenomenon was utilized by the Somorjai group to explain the enhanced activity of $Co/TiO_2$ in comparison with $Co/SiO_2$ for $CO_2$ hydrogenation.[6] Very recently, Zhao et al. employed analytical electron microscopy analysis similar to our own to demonstrate that a 20-fold increase in activity for propene hydrogenation is due to Ir spreading over $TiO_2$ through a strong metal−support interaction.[39] As with this previous report, in our case we cannot conclusively state if the influence on activity is purely morphological or has some electronic contribution. However, we can conclude that both atomic Pt decoration of Co and spreading of Co on the support material do lead to an enhanced activity and selectivity in $CO_2$ methanation.

$Y^{3+}$ doping of the $BaZrO_3$ support to provide insights for possible proton incorporation into the support material is, in this case, found to be detrimental to the overall rate of $CO_2$ methanation. This is perhaps in contrast to the previous reports proposing that H transport between the Co and Pt particles is essential to the catalytic mechanism.[16−18] One possible explanation is that the intimate decoration of Co with Pt in our catalysts avoids this H-transport requirement, as it facilitates direct spillover from Pt to Co. Alternatively, it may be that bulk proton incorporation leads to some depletion of hydrogen available for the desired reaction. We previously reported that ethane dehydrogenation rates catalyzed by Cr supported on metal oxides are also enhanced when utilizing a $BaZrO_3$ or $BaCeO_3$ support in comparison with $Al_2O_3$.[21] Clearly these materials are promising support materials for a range of supported metal catalysts, but the question of a possible role for proton incorporation in the reaction mechanism remains unclear and will most likely show a complex interdependency on metal−support interactions, the support material composition and structure, and the precise reaction conditions.

## CONCLUSIONS

The use of $BaZrO_3$ as a support significantly enhances a Pt and Co nanoparticle cooperative catalytic mechanism for $CO_2$ hydrogenation. Co catalyzes the dissociation of $CO_2$, with hydrogen dissociation occurring primarily on Pt. The most active catalyst structure consists of Co nanoparticles on a $BaZrO_3$ support, with both the Co and $BaZrO_3$ support surface decorated with highly dispersed Pt atoms. This structure is formed, by migration and spreading of Pt atoms from small (~2.5 nm) Pt nanoparticles, during initial elevated temperature

calcination and reduction of the material. This catalyst leads to a 6-fold increase in $CH_4$ production rate, accompanied by a high $CH_4$ selectivity, in comparison what is obtained using γ-$Al_2O_3$ as the support. The primary deactivation mechanism for this catalyst is carbon formation. This work clearly demonstrates that there is considerable scope for further catalyst design and optimization for this important class of $CO_2$ hydrogenation catalyst.

## AUTHOR INFORMATION


### Corresponding Author

*E-mail for S.M.: mcintosh@lehigh.edu.


### Notes

The authors declare no competing financial interest.

## ACKNOWLEDGMENTS


The authors are grateful to Ryan Thorpe at Rutgers University for assistance with XPS measurements. Support for this work was received from Lehigh University with additional partial support from the National Science Foundation under the EFRI-PSBR program (Grant No. 1332349).


## REFERENCES


(1) Ritter, S. K. Chem. Eng. News 2007, 85, 11−17.
(2) Schwartz, S. E. Energy Environ. Sci. 2008, 1, 430−453.
(3) Centi, G.; Quadrelli, E. A.; Perathoner, S. Energy Environ. Sci. 2013, 6, 1711−1731.
(4) Watson, G. H. Methanation Catalysis. In International Energy Agency Coal Research; International Energy Agency: London, 1980; pp 1−56.
(5) Alayoglu, S.; Beaumont, S. K.; Zheng, F.; Pushkarev, V. V.; Zheng, H.; Iablokov, V.; Liu, Z.; Guo, J.; Kruse, N.; Somorjai, G. A. Top. Catal. 2011, 54, 778−785.
(6) Melaet, G.; Ralston, W. T.; Li, C.; Alayoglu, S.; An, K.; Musselwhite, N.; Kalkan, B.; Somorjai, G. A. J. Am. Chem. Soc. 2014, 136, 2260−2263.
(7) Zhang, Y.; Jacobs, G.; Sparks, D. E.; Dry, M. E.; Davis, B. H. Catal. Today 2002, 71, 411−418.
(8) Wang, W.; Wang, S.; Ma, X.; Gong, J. Chem. Soc. Rev. 2011, 40, 3703−3727.
(9) Khodakov, A. Y.; Chu, W.; Fongarland, P. Chem. Rev. 2007, 107, 1692−1744.
(10) Schanke, D.; Vada, S.; Blekkan, E. A.; Hilmen, A. M.; Hoff, A.; Holmen, A. J. Catal. 1995, 156, 85−95.
(11) Bell, A. T. Science 2003, 299, 1688−1691.
(12) Qiao, B.; Wang, A.; Yang, X.; Allard, L. F.; Jiang, Z.; Cui, Y.; Liu, J.; Li, J.; Zhang, T. Nat. Chem. 2011, 3, 634−641.
(13) Thomas, J. M.; Raja, R.; Lewis, D. W. Angew. Chem., Int. Ed. 2005, 44, 6456−6482.
(14) Yang, X.; Wang, A.; Qiao, B.; Li, J.; Liu, J.; Zhang, T. Acc. Chem. Res. 2013, 46, 1740−1748.
(15) Thomas, J. M.; Saghi, Z.; Gai, P. L. Top. Catal. 2011, 54, 588−594.
(16) Iablokov, V.; Beaumont, S.; Alayoglu, S.; Pushkarev, V.; Specht, C.; Gao, J.; Alivisatos, A. P.; Kruse, N.; Somorjai, G. A. Nano Lett. 2012, 12, 3091−3096.
(17) Beaumont, S. K.; Alayoglu, S.; Specht, C.; Michalak, W. D.; Pushkarev, V. V.; Guo, J.; Kruse, N.; Somorjai, G. A. J. Am. Chem. Soc. 2014, 136, 9898−9901.
(18) Beaumont, S. K.; Alayoglu, S.; Specht, C.; Kruse, N.; Somorjai, G. A. Nano Lett. 2014, 14, 4792−4796.
(19) Iwahara, H.; Yajima, T.; Hibino, T.; Ozaki, K.; Suzuki, H. Solid State Ionics 1993, 61, 65−69.
(20) Shin, H. H.; McIntosh, S. J. Mater. Chem. A 2013, 1, 7639.
(21) Shin, H. H.; McIntosh, S. ACS Catal. 2015, 5, 95−103.
(22) Wang, C.; Daimon, H.; Lee, Y.; Kim, J.; Sun, S. J. Am. Chem. Soc. 2007, 129, 6974−6975.
(23) Vogel, A. Textbook of Quantitative Inorganic Analysis; Longman Scientific and Technical: Harlow, United Kingdom, 1986.
(24) Levy, P.; Primet, M. Appl. Catal. 1991, 70, 263−276.
(25) Stokes, S. J.; Islam, M. S. J. Mater. Chem. 2010, 20, 6258−6264.
(26) Braun, A.; Duval, S.; Ried, P.; Embs, J.; Juranyi, F.; Strassle, T.; Stimming, U.; Hempelmann, R.; Holtappels, P.; Graule, T. J. Appl. Electrochem. 2009, 39, 471−475.
(27) Duval, S. B. C.; Holtappels, P.; Vogt, U. F.; Stimming, U.; Graule, T. Fuel Cells 2009, 9, 613−621.
(28) Tao, S.; Irvine, J. T. S. J. Solid State Chem. 2007, 180, 3493−3503.
(29) Kreuer, K. D.; Adams, S.; Munch, W.; Fuchs, A.; Klock, U.; Maier, J. Solid State Ionics 2001, 145, 295−306.
(30) Kreuer, K. D. Annu. Rev. Mater. Res. 2003, 33, 333−359.
(31) Buffat, P.; Borel, J. B. Phys. Rev. A: At., Mol., Opt. Phys. 1976, 13, 2287−2298.
(32) Nanda, K. K.; Sahu, S. N.; Behera, S. N. Phys. Rev. A: At., Mol., Opt. Phys. 2002, 66, 013208.
(33) Tauster, S. J.; Fung, S. C.; Baker, R. T.; Horsley, J. A. Science 1981, 211, 1121−1125.
(34) Stakheev, A. Y.; Kustov, L. M. Appl. Catal., A 1999, 188, 3−35.
(35) Gonzalez-DelaCruz, V. M.; Holgado, J. P.; Pereñíguez, R.; Caballero, A. J. Catal. 2008, 257, 307−314.
(36) Farmer, J. A.; Campbell, C. T. Science 2010, 329, 933−936.
(37) Tauster, S. Acc. Chem. Res. 1987, 20, 389−394.
(38) Riva, R.; Miessner, H.; Vitali, R.; Del Piero, G. Appl. Catal., A 2000, 196, 111−123.
(39) Zhao, E. W.; Zheng, H.; Ludden, K.; Xin, Y.; Hagelin-Weaver, H.; Bowers, C. R. ACS Catal. 2016, 6, 974−978.